



# High resolution grating-assisted surface plasmon resonance fiber optic aptasensor



Jacques Albert<sup>a,\*</sup>, Sandrine Lepinay<sup>a</sup>, Christophe Caucheteur<sup>b</sup>, Maria C. DeRosa<sup>c</sup>

<sup>a</sup> Department of Electronics, Carleton University, 1125 Colonel By Drive, Ottawa, Ontario K1S5B5, Canada

<sup>b</sup> Electromagnetism and Telecom Unit, Université de Mons, 31 Boulevard Dolez, Mons 7000, Belgium

<sup>c</sup> Department of Chemistry, Carleton University, 1125 Colonel By Drive, Ottawa, Ontario K1S5B5, Canada

## ARTICLE INFO

### Article history:

Available online 17 July 2013

### Keywords:

Surface plasmon resonance  
Fiber sensor  
Aptamer  
Fiber grating  
Biochemical sensor

## ABSTRACT

A surface plasmon resonance biochemical sensor based on a tilted fiber Bragg grating imprinted in a single mode fiber core is demonstrated. A 30–50 nm thick gold coating on the cladding of the fiber provides the support for surface plasmon waves whose interaction with attached biomolecules is monitored at near infrared wavelengths near 1550 nm. The transmission spectrum of the sensor provides a fine comb of narrowband resonances that overlap with the broader absorption of the surface plasmon and thus provide a unique tool to measure small shifts of the plasmon with high accuracy. The attachment on the gold surfaces of aptamers with specific affinities for proteins provides the required target-analyte system and is shown to be functional in the framework of our sensing device. The implementation of the sensor either as a stand-alone device or as part of a multi-sensor platform is also described.

© 2013 Elsevier Inc. All rights reserved.

## 1. Introduction

In recent years, biochemical sensors relying, for their detection process, on the interaction of light with molecules ranging from simple to complex have become commonplace. In all cases a probe light beam with suitable properties is directed at a sample, or at an array of samples, and its reflection or transmission is monitored as a function of various parameters. Changes in the properties of the molecules and substances being probed lead to corresponding modification of the optical transfer function of the devices. The parameter changes that are routinely detected include those arising from chemical reactions, biomolecular binding processes and simply size or spatial distribution modifications [1–4]. In all cases, the use of optics enables high sensitivity detection because of three important factors:

- (1) light consists of a high frequency wave whose exact phase can easily be determined (with an interferometer for instance);
- (2) waves of different frequencies (“colours”) can propagate simultaneously in the same volume of space without interfering (thereby allowing for wavelength multiplexing and demultiplexing, including pump–probe experiments);
- (3) light beams can be shaped or directed in space to probe multiple detection points simultaneously (this allows parallel processing and the use of arrays of samples).

In order to benefit fully from any or all of these factors, the most sensitive optical sensing systems rely on complex arrangements of light sources, optical elements (lenses, prisms, polarizers, diffraction gratings, mirrors) and detectors, associated with good electronic systems to maximize the signal-to-noise ratio (SNR) and allow for reference channels to eliminate background effects [5–7].

In parallel with these advances, much effort has been devoted toward the development of optical biosensors using optical fibers to deliver and/or collect light. The use of fiber removes many constraints in getting the light to and from samples, but at the same time limits the kinds of interaction that can be achieved on samples, unless the light is taken out of the fiber prior to reaching the sensing volume or surface. Therefore, it has been generally acknowledged that intrinsic fiber optic sensors (i.e. those kinds of sensors for which light remains guided, or partially guided by the fiber as it interacts with molecules and materials) have limited performance compared to bulk optic counterparts, but remain relevant in applications where their small size and remote operability make a difference [8–11].

In the work presented here, we demonstrate a fiber-based surface Plasmon resonance sensor whose performance approaches that of bulk optic counterparts. This device is unique because it uses a fine comb of spectral resonances whose sensitivity to events occurring on the fiber surface is highly differentiated. This differentiation is amplified by plasmonic effects due to the presence of a thin gold coating on the fiber surface. Measurements with those sensors involve comparing the spectral changes of several individual resonances, including reference “channels” and a temperature monitor (all from a single device), for the highly sensitive detection of

\* Corresponding author.

E-mail addresses: [jacques\\_albert@carleton.ca](mailto:jacques_albert@carleton.ca) (J. Albert), [Christophe.Caucheteur@umons.ac.be](mailto:Christophe.Caucheteur@umons.ac.be) (C. Caucheteur), [maria\\_derosa@carleton.ca](mailto:maria_derosa@carleton.ca) (M.C. DeRosa).

biomolecular binding events on the fiber surface. The high sensitivity and low limit of detection (LOD) arise because when used at near infrared wavelengths between 1.5 and 1.6  $\mu\text{m}$ , the spectral width of the resonances of our sensors lie between 0.01 and 0.1 nm for Q-factors as high as  $10^5$  (with the Q-factor defined as wavelength/spectral width at half maximum). A high Q-factor is an important factor in the sensitivity of resonant sensing devices as it helps to measure small wavelength shifts with greater accuracy [4]. Furthermore, we use standard single mode telecommunication grade optical fiber with propagation loss under 0.2 dB/km at these wavelengths. Finally, this high transparency and the widespread availability of powerful, low-noise light sources and detectors developed especially for these kinds of fibers mean that it is very straightforward to develop interrogation systems with a dynamic range exceeding 50 dB (thereby completing the requirements for low LOD: narrow resonances, high sensitivity, and low noise). In comparison to other demonstrated fiber based SPR sensors [12–14], we use a short period grating photo-inscribed in the core of the single mode fiber to retrieve very precise phase information from the light propagating in the fiber. The grating also couples some of the light from the low loss fiber core to the cladding, where it can interact with the gold coating without having to mechanically remove the cladding or otherwise perturb the fiber to allow such contact (Fig. 1).

Finally, amongst the many possible coatings developed to perform molecular recognition experiments on the surface of the gold covered fibers, we have chosen to use aptamers as our molecular receptors. Aptamers are single stranded DNA or RNA that fold into selective, high affinity binding pockets for a target molecule. They are discovered using an *in vitro* process called Systematic Evolution of Ligands by EXponential enrichment (SELEX), a procedure where target-binding DNA or RNA are selected from a random library of sequences through iterative cycles of affinity separation and amplification [15]. Aptamer generation has been achieved for a wide variety of targets including small molecules [15], proteins [16], viruses [17] and whole cells [18]. Aptamers have several advantages over antibodies, which have long been considered the standard in molecular recognition, that have led to their emergence as a viable alternative for biosensing applications. Firstly, the *in vitro* aptamer selection process allows a greater control over aptamer binding conditions. Non-physiological salt concentrations, temperatures and pH can be used in successful selections, allowing for aptamers to be better tailored to their eventual sensing environment. Due to the robustness of the DNA phosphodiester backbone, aptamers can exhibit an extended shelf life over their

protein-based antibody counterparts. In particular, aptamers can be reversibly denatured by changing the surrounding conditions. For example, a change in pH, temperature, ionic strength or use of chaotropic agents irreversibly denatures antibodies, while aptamers simply unfold. The aptamer structure can then regain functionality upon return of the original binding conditions. Unlike antibodies, aptamers can also be generated for targets that are toxic as well as for targets that do not elicit an immune response *in vivo*. Once selected, aptamers are manufactured using well-established automated chemical solid-phase synthesis [19]. The accuracy and reproducibility of this procedure allows for a relative ease in producing aptamers at large scales, with very little batch-to-batch variation in activity. Additionally, aptamer sequences can be modified with reporter molecules throughout this solid-phase synthesis; this allows for labeling at judiciously chosen nucleotide positions to minimize any effect on the functionality of the aptamer. Moreover, this opens up a range of surface conjugation chemistries for biosensing [20].

The paper is organized as follows. The sensor platform and its function are described in detail in Section 2, which is followed by Sections 3 and 4 which deal respectively with the fabrication of the sensor probe and its functionalization with biomolecules. Section 5 describes the sensor interrogation process and the instrumentation required. Finally some representative biochemical binding experiments are reported in Section 6, which is followed by a short conclusion on the potential and the limits of this new approach.

## 2. Description of the basic sensor

The sensor device consists of a single mode optical fiber in which a photoimprinted refractive index grating has been formed over a short section of the core, and that is further provided with a two layered coating: a very thin metal coating and a suitable biochemical recognition binding layer.

The glass optical fiber is a 125  $\mu\text{m}$ -thick cylindrical waveguide made of two concentric layers, the core in the middle surrounded by a cladding that is thick enough to isolate the light propagating in the core from interacting with the fiber surroundings. To allow for the guidance of light in the fiber core, the refractive index of the core is slightly higher than that of the cladding. Our experiments are conducted on single-mode optical fibers characterized by a core diameter of 8 microns that guides light into a single optical mode (or trajectory) at wavelengths between 1300 nm and 1650 nm. We use CORNING SMF-28 fiber but any fiber complying with the ITU-T G.652.D international standard (which specifies the physical and optical properties of optical fibers for telecommunications) would work just as well. These fibers are widely available at low cost (less than 100 US\$/km) because they are used for much of the telecommunications infrastructure deployed globally. For the same reason, a large quantity of equipment is available to characterize, manipulate and use such fibers and devices made from them (such as splitters, connectors, polarizers, etc...). The specific equipment used in our work will be specified in Section 5.

As sketched in Fig. 2a, a uniform fiber Bragg grating (FBG) is a periodic and permanent refractive index modulation of the fiber core that is imprinted perpendicularly to the propagation axis [21,22]. It behaves as a selective mirror in wavelength for the light propagating in the core, reflecting a narrow spectral band centered on the so-called Bragg wavelength  $\lambda_{\text{Bragg}} = 2n_{\text{eff,core}}\Lambda$  where  $n_{\text{eff,core}}$  is the effective refractive index of the core mode (close to 1.45) and  $\Lambda$  is the grating periodicity (the effective index of a mode is a measure of its phase velocity  $v_p = c/n_{\text{eff,core}}$ , where  $c$  is the speed of light in vacuum). In practice,  $\Lambda \sim 500$  nm to ensure that the Bragg wavelength falls in the band of minimum attenuation of the optical

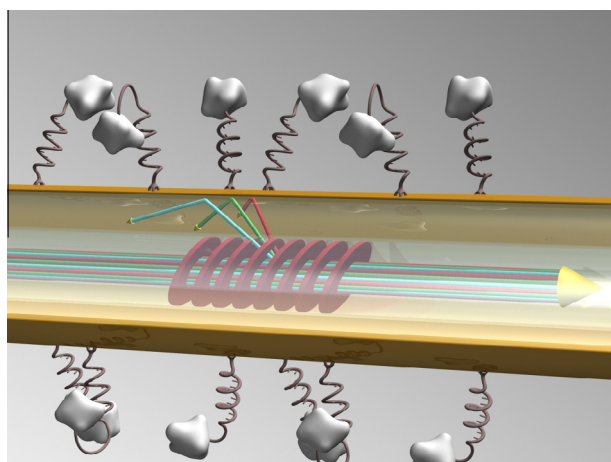


Fig. 1. Schematic diagram of gold coated tilted fiber Bragg grating surface plasmon resonance sensor coated with aptamer receptor molecules.

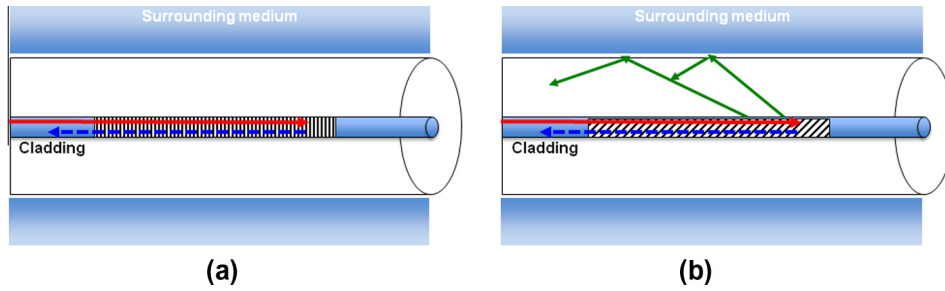


Fig. 2. Sketch of the light coupling mechanism for uniform FBGs (a) and tilted FBGs (b).

fiber centered on 1550 nm. The Bragg wavelength is inherently sensitive to mechanical strain and temperature, through a change of both  $n_{\text{eff}}$  and  $\Lambda$  [21]. For instance a change of temperature of +1 °C shifts a Bragg resonance located near 1550 nm by 0.01 nm. Such change is easily measured with standard telecommunication instruments since the full spectral width of the reflected light from a typical 1 cm-long grating is of the order of 0.1 nm. However our purpose here is to measure events occurring on or near the fiber cladding surface and the core mode reflection spectrum is inherently and totally insensitive to such changes (because the penetration depth of core guided light into the cladding does not exceed a few micrometers). We use a small modification of the FBG to couple light from the core to the cladding and still benefit from narrowband spectral resonances that will reveal small changes at the cladding boundary.

A tilted fiber Bragg grating (TFBG) corresponds to a refractive index modulation angled by a few degrees relative to the perpendicular to the propagation axis (Fig. 2b) [23]. The properties and features of TFBG sensors have recently been reviewed extensively [11] so only the main results will be reproduced here. In addition to the self-backward coupling of the core mode at the Bragg wavelength, the grating now redirects some light to the cladding whose diameter is so large that several possible cladding modes can propagate, each with its own phase velocity (and hence effective index  $n_{\text{eff,clad}}$ ). These possible modes of propagation correspond to different ray angles in Fig. 2b. Again there is a one-to-one relationship between the wavelength at which coupling occurs for a given cladding mode and its effective index. This relationship is expressed by a similar phase matching condition as before:  $\lambda_{\text{clad}} = (n_{\text{eff,core}} + n_{\text{eff,clad}})\Lambda$  where the index “i” reflects the fact that the fiber cladding can support many modes. Fig. 3 shows a TFBG transmission spectrum where each dip corresponds to the coupling from the core mode to a group of backward propagating cladding modes. As a result of phase matching, the spectral position of a resonance now depends on the effective index of its associated cladding mode, which in turn depends on the optical properties of the medium on or near the cladding surface.

Therefore, spectral shifts of individual resonances can be used to measure changes in fiber coatings and surroundings. But another factor comes into play in this case because the strength of the coupling for a particular resonance (cladding mode) depends on the distribution and polarization of the electromagnetic field of the mode over the fiber cross-section. For instance when the surrounding refractive index (SRI) increases, the mode field becomes less confined by the cladding and extends deeper outside of the fiber: this generally results in a decrease of the coupling strength because a smaller fraction of the mode field remains in the vicinity of the core to participate in the coupling process. The coupling strength is a quantity that can be measured with great precision as will be shown in Section 3.

Laffont and Ferdinand were the first to demonstrate SRI sensing with TFBGs in 2001 [24]. They observed a progressive smoothing of

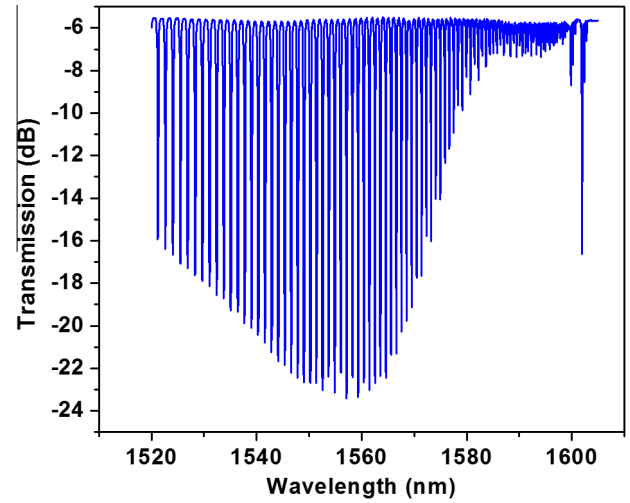


Fig. 3. Typical transmission spectrum of a 10° tilted fiber Bragg grating measured in air (using linearly polarized input light as described in Section 5).

the transmitted spectrum starting from the shortest wavelengths as the SRI increased from 1.30 to 1.45. Several data processing techniques can be used to quantitatively correlate the spectral content with the SRI value, either based on a global spectral evolution or a local spectral feature change. The first method involves monitoring the area delimited by the cladding mode resonance spectrum, through a computation of the upper and lower envelopes as resonances gradually disappear when the SRI reaches the cut-off points of each cladding mode [24,25]. Another technique tracks the wavelength shift and amplitude variation of individual cladding mode resonances as they approach cut-off [26]. Both techniques present minimum detectable SRI changes of  $\sim 10^{-4}$  RIU (refractive index unit). In terms of wavelength tracking, this result is obtained with a sensitivity that peaks between 10 and 15 nm/RIU for the modes near cut-off. In all cases, the Bragg wavelength provides an absolute power and wavelength reference which can be used to remove uncertainties related to systematic fluctuations (such as power level changes from the light sources) and even temperature changes (because it was demonstrated in Chen et al. [27] that all resonances shift by the same amount when the temperature changes). The TFBG thus allows inherently temperature-insensitive SRI measurements and large signal-to-noise ratio.

For biochemical experiments however, it is usually necessary to improve the LOD levels to at least  $10^{-5}$  RIU, by increasing the wavelength shift sensitivity while keeping noise level down and spectral features narrow [28]. Fortunately, it has been recently demonstrated that the addition of a nanometric-scale gold coating overlay on the TFBG outer surface considerably enhances the refractometric sensitivity through the generation of surface plasmon resonances (SPR) [29–31]. In simplified terms, surface

plasmons are electromagnetic waves that are confined to the interface between a metal and a dielectric. These waves have a well-defined phase velocity that depends solely on the frequency of the wave, and on the complex refractive indices of the metal and the dielectric. Furthermore plasmons are polarized at right angles to the metal surface (i.e. radially for metal coatings on cylindrical fibers). The increased sensitivity achieved with plasmon waves arises because of the large localization of electromagnetic energy in the layer immediately adjacent to the metal surface. Any perturbation in that layer, such as the binding of analytes on receptor molecules modifies the local refractive index of the dielectric and the plasmon phase velocity. In order to excite and measure plasmon resonances and hence to achieve this optimum sensitivity, we use two unique features of TFBGs: (1) the polarization selectivity that comes about from the breaking of the cylindrical symmetry of our non-polarization-maintaining fibers, and (2) the high-density comb of narrowband spectral resonances that are available to excite SPR and to measure their spectral location (with quality factors between  $10^3$  and  $10^4$ ). These features are described in detail in the following paragraph.

In contrast with conventional FBGs, the tilt angle breaks the cylindrical symmetry of the coupling mechanism relative to the state of polarization (SOP) of the input core guided light. Input light linearly polarized in the plane of the tilt (P-polarization) couples to different cladding modes than light polarized perpendicularly to it (S-polarization). In the former case, high order cladding modes have their electric field polarized mostly radially at the cladding-metal boundary while for the orthogonal input polarization the cladding modes are azimuthally polarized (hence tangential to the metal surface). In addition to phase velocity matching between the cladding mode and the plasmon wave, this transfer of energy can only occur when the electric field polarization of the mode is aligned perpendicularly to the coating surface, i.e. radially. Therefore, P-polarized input light alone can lead to a very efficient transfer of energy from the core mode to a specific cladding mode and then to a surface plasmon wave on the outer surface of the nano-scale metal layer coating. The successful transfer of energy between a given cladding mode and the plasmon wave is identified by a pronounced decrease of the amplitude of this cladding mode resonance in the TFBG transmission spectrum, as reported in [30]. Under these conditions, very small changes occurring in a 1–2  $\mu\text{m}$  thick layer on top of the metal surface lead to strong modifications of the plasmon wave properties and can be monitored precisely by following the spectral transmission of the associated cladding mode resonances [31]. On the other hand, S-polarized light does not tunnel efficiently through the metal and associated cladding modes remain unaffected by plasmon wave effects. This behavior is depicted in Fig. 4 that presents two orthogonal amplitude transmitted spectra for a gold-coated TFBG immersed in water (fabrication and measurement techniques are described in the following section). A pronounced amplitude decrease locally occurs for the P spectrum for cladding mode resonances whose effective index corresponds to the one of the Plasmon wave (cf. inset of Fig. 4).

The sensing mechanism works as follows: the binding between analyte and receptor molecules on the gold surface changes the phase velocity of the plasmon wave and hence the wavelength of the most attenuated cladding mode shifts. Sensing over a large range is possible by tracking the wavelength shift of the center of the envelope of the most attenuated resonances in a P-polarized spectrum (labeled “SPR” in the inset of Fig. 4). This results in a SRI sensitivity of  $\sim 500$  nm/RIU in a range of SRI from 1.32 to 1.42, i.e. at least 20 times larger than for non-plasmon-assisted refractometry and similar in magnitude to bulk optic SPR sensors such as Kretschmann type instruments [2]. The sensitivity is given in terms of refractive index units for comparison with other SPR sensor platforms (in biochemical sensing, the amount of index change

associated with binding events varies widely with the types of molecules involved). However the limit of detection (in this case associated with the smallest detectable wavelength shift) is not very good because the center of the SPR attenuation is not well defined in the spectrum (near 1550 nm in Fig. 4). This particular problem also exists in bulk instruments where it is addressed by very careful handling of optical and electrical noise sources and by using reference channels. In TFBGs, a fine comb of narrowband resonances samples the envelope of the SPR attenuation and this can be used to increase the resolution. However the cladding mode resonance that is most closely phase matched to the SPR and hence most sensitive is so attenuated that it becomes impossible to detect. A more efficient interrogation technique consists in monitoring the evolution of a selected resonance located slightly away from the SPR center, near 1545 nm in the spectrum of Fig. 4 for instance. These resonances are only partly attenuated by the SPR effect so that they retain a significant amplitude (10–15 dB) and remain narrowband. Because of their location on the shoulder of the SPR envelope the main effect of small spectral shifts of the SPR is to increase or decrease the resonance amplitudes depending on the direction of the SPR shift, as shown schematically on Fig. 5. The location of the most sensitive resonance is shown as  $\lambda_S$  on Fig. 4.

There are two ways to utilize this effect to achieve high resolution detection: either by monitoring the amplitude changes of selected resonances on the SPR shoulder; or by using the “Polarization Dependent Loss” or PDL which combines the transmission spectra of the S- and P-polarized into a single graph. We will concentrate on the amplitude change method in this paper (Sections 4–6) but we have shown earlier that the PDL spectrum contains narrowband (near 50 pm wide) resonant features on the short wavelength side of the SPR maximum that can be tracked to enable refractive index change LOD of  $10^{-5}$  RIU, achieved through a quality factor (resonance wavelength divided by full width at half maximum) of  $10^5$  and signal-to-noise ratio greater than 50 dB [32,33].

### 3. Fabrication of the optical fiber sensor

The sensor probe itself consists of the fiber grating and of the gold coating to which biomolecules will be attached. For gratings, a well established technological base exists and they are quite easy to fabricate in large quantities, even in modestly equipped facilities. However the preparation of good quality gold layers at the required thicknesses (between 30 and 50 nm) is a little more difficult, especially given the need for relative uniformity around the circumference of the 125  $\mu\text{m}$  diameter of the fiber.

#### 3.1. Fabrication of TFBGs

TFBGs are manufactured in the same way as conventional FBGs, i.e. through a lateral illumination of the fiber core using an interference pattern of ultraviolet (UV) light between 190 and 260 nm. The exposure of the fiber to bright interference fringes for a few minutes locally and permanently increases the mean refractive index of the core. The ultraviolet interference pattern is reproduced inside the fiber much like in a photographic process. Mass production of identical gratings is straightforward when the phase mask technique is used to generate the interference pattern. A phase mask is a diffractive element made in a pure silica substrate that is optimized to maximize the diffraction in the first (+1 and –1) diffraction orders [21]. An interference pattern at half the period of the mask is therefore produced in the fiber core when the optical fiber is located in close proximity behind the mask. Because of the well established FBG manufacturing base, there are several phase mask suppliers

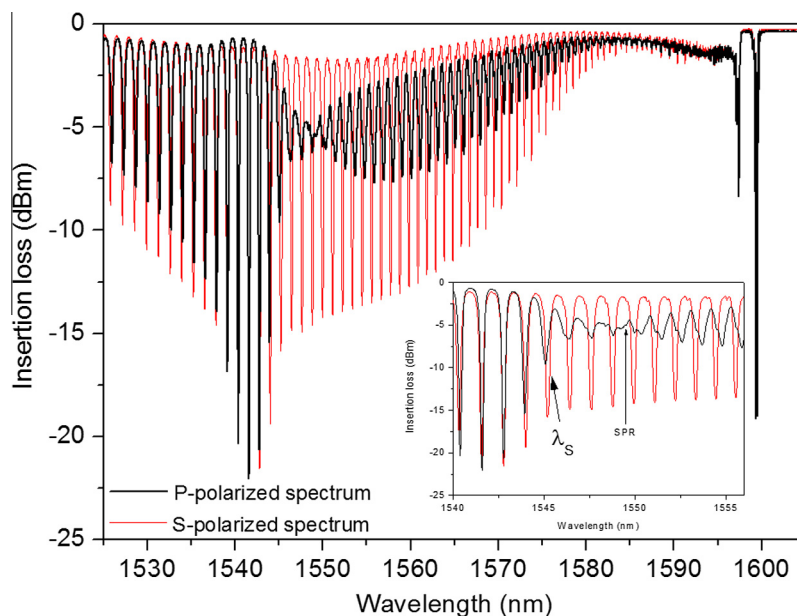


Fig. 4. Polarized transmission spectra of a gold coated TFBG in water.

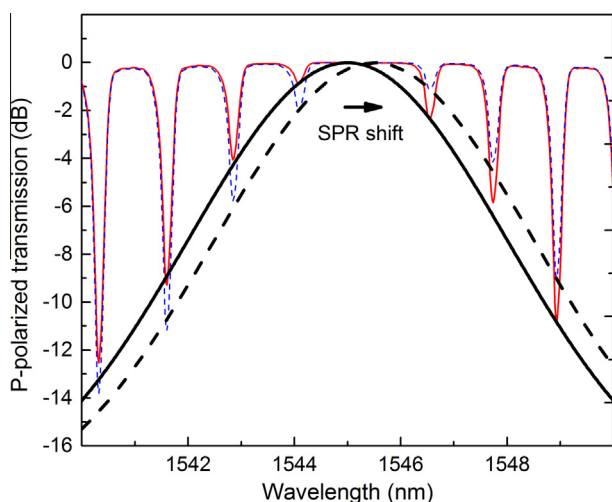


Fig. 5. Illustration of how the shift of the SPR envelope (thick curves) introduces amplitude changes in the neighboring TFBG resonances in the transmission spectra (thin lines).

including Ibsen Photonics and Coherent Inc., and the only parameters to be specified are the size of the mask (length and height of the diffractive pattern on the mask), the ultraviolet wavelength at which the mask is to be used (this determines the groove depth for optimum diffraction into the  $\pm 1$  orders), and the mask period. In the fibers that we use, a mask period of 1112 nm yields a Bragg wavelength of 1610 nm. In order to obtain a “tilted” FBG, the interference pattern must be rotated relatively to the fiber axis. There are two ways to do this: (1) rotating both the fiber and the phase mask in the incidence plane of the UV laser beam (Fig. 6a) or (2) rotating only the phase mask in the plane perpendicular to the UV laser beam (Fig. 6b). Although the second method is somewhat simpler to setup, we use the method of Fig. 6a as it offers a flatter interference pattern inside the fiber and consistently produces TFBGs with strong and narrow cladding mode resonances.

We work with a pulsed high-energy excimer laser (model PM-848 from Light Machinery Inc.) operating at 248 nm with an energy per pulse adjustable between 100 and 400 mJ and a fixed beam size of  $10 \times 40$  mm. The pulse repetition rate is adjustable

from single shot to 100 Hz and has no impact on the TFBGs, apart from the speed of inscription. Other intense ultraviolet sources can be used, including smaller frame excimer laser such as the “Bragg-star” (Coherent Inc.) developed especially for FBG manufacture. The advantage of a more powerful excimer laser rests with the fact that the beam can be expanded laterally by a large factor (up to  $20\times$  at least) and still retain enough energy density ( $10\text{--}40$  mJ/cm at the fiber) to write strong gratings as long as 15 cm in a single exposure lasting less than 5 min (the same gratings written with less powerful lasers require scanning the beam over the grating length and much longer exposures). In order to maintain enough energy density on the fiber, a 15 cm focal length cylindrical lens at least as long as the grating to be written is used to concentrate the widened ultraviolet laser beam to a fine line (about  $10\ \mu\text{m}$  in height) along the fiber axis, just behind the phase mask.

We routinely produce TFBGs with tilt angles varying between  $4^\circ$  and  $10^\circ$ , the larger angle being preferred for work when the SRI lies near the index of water and water solutions, which is often the case in biochemical research, because then the strongest cladding mode resonances are located near 1550 nm (when the Bragg wavelength is near 1610 nm), where they are easier to measure. Prior to the manufacturing process, the single-mode fibers are hydrogen-loaded (by soaking for 10 days in a vessel containing pure hydrogen at a pressure of 14 MPa) to enhance their photosensitivity to ultraviolet light [34].

The end product (the TFBG), consists of an invisible periodic refractive index modulation of the transparent core of the optical fiber, with a periodicity of the order of 500 nm, typical lengths between 1 and 2 cm. The  $125\ \mu\text{m}$ -diameter cylindrical cross-section of the optical fiber is not modified by this process.

### 3.2. Fabrication of the gold coating

#### 3.2.1. RF sputtering

The gold overlay can be successfully deposited using well-established technologies, such as electroless deposition, electroplating or sputtering. The latter is used more routinely and yields very high quality gold surfaces. We use a Polaron Instruments model E5100 sputtering chamber in the following conditions: the primary vacuum is set to a pressure of 13 Pa and the arc discharge

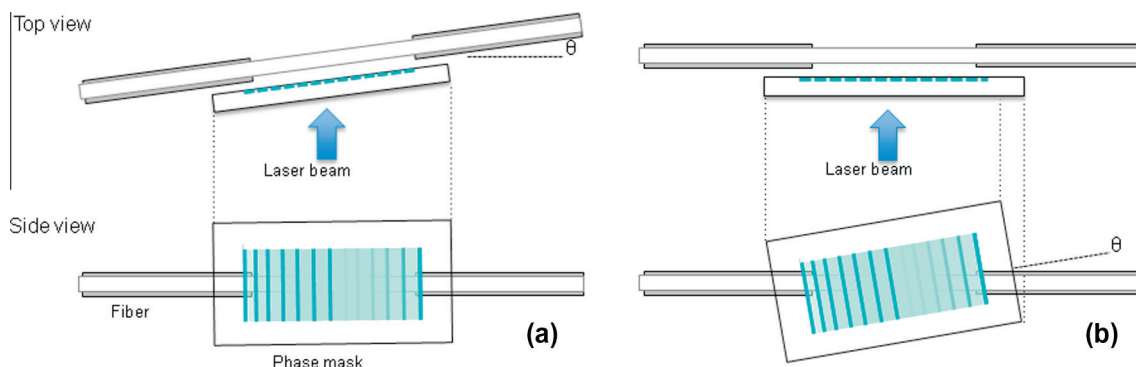


Fig. 6. (a) and (b) illustrate two variants on the configuration used to manufacture TFBGs in optical fiber. We use configuration (a).

current is set between 18 and 20 mA at a potential difference of 2.5 kV to extract gold from a 99.99% purity target. Two consecutive depositions are made in the same conditions, with the optical fibers rotated by 180° between both processes, to ensure that the whole outer surface is covered by gold. The optimum gold thickness has been found to be approximately 50 nm, for the narrowest, deepest SPR attenuation. In spite of the two-step deposition which yields a slightly non-uniform thickness around the fiber circumference, we did not find this non-uniformity to be detrimental for SPR generation in practice. Also, as the vacuum is obtained in the chamber starting from ambient air and not from an inert (Argon) starting atmosphere, there is no need for a 2–3 nm thick adhesion layer of Chromium or Titanium between the silica surface and the gold coating.

### 3.2.2. Electroless deposition

Electroless deposition is another technique that we have used for gold and silver films. This technique is based on the reduction of metallic ions from a solution to a solid surface without electrical potential [35]. The electroless deposition requires several steps. First of all, the plastic coating protecting the fiber is removed by soaking it into dichloromethane ( $\text{CH}_2\text{Cl}_2$ ). Then, the uncoated area of the fiber is rinsed with methanol and subsequently treated with a freshly prepared piranha solution ( $\text{H}_2\text{SO}_4/\text{H}_2\text{O}_2 = 3:1$ ) for 20 min followed by rinsing with de-ionized water. This strong cleaning process allows for the formation of hydroxyl groups ( $\text{Si-OH}$ ) at the surface but according to the literature, the modification of silica surfaces is more stable when a silanization procedure is carried out [36,37]. Thus, the cleaned fiber is immersed in a solution of 4-aminopropyltrimethoxysilane (APTMS, 1% in methanol) for 20 min and then rinsed with methanol, de-ionized water and finally dried with nitrogen gas. The result is a surface coated with a self assembled monolayer (SAM) with exposed amine groups at the end. Once dry, the modified fiber is dipped into a colloidal solution of gold nanoparticles for 24 h. These gold nanoparticles interact with the amine groups at the surface to form multiple chemical bonds. The actual electroless deposition is now ready to proceed. The fiber coated with gold nanoparticles is immersed into an aqueous plating solution containing a complex metal ions solution (2% in weight of chloroauric acid,  $\text{HAuCl}_4$ ) and a reducing agent solution (0.8 mM hydroxyl amine hydrochloride,  $\text{NH}_2\text{OHCl}$ ). The fiber is left in the solution for 20 min without stirring. The hydroxylamine hydrochloride reduces the gold nanoparticles immobilised on the surface to form bigger nanoparticles until a somewhat continuous thin gold film is formed. Of particular interest in this context is that the electroless process used to form a metal film on a TFBG sensor can be followed in real time by interrogating the TFBG while it gets plated as demonstrated in [38].

## 4. Functionalization of the sensor for biochemical applications

This Section begins with an overview of techniques that can be used to bind biomolecules on gold surfaces, and therefore that can be applied to our sensing device. Then the specific case of aptamer-based functional coatings is described in more details.

### 4.1. Immobilization of biomolecules on gold

A critical element in the design of our biosensor is the approach used for the immobilization of receptor biomolecules on the sensor surface. Most methods fall in one of two categories, broadly characterized as either physical or covalent immobilization (Fig. 7).

#### 4.1.1. Direct physical immobilization of the receptor biomolecules on the gold substrate

In this simple approach, there is no conjugation chemistry linking the receptor directly to the gold surface, rather the aim is to adsorb the biomolecule onto the substrate's surface. While the nature of the physical interaction during the adsorption process is not completely understood, in the case of biomolecule adsorption on gold it is thought that hydrophobic interactions dominate this kind of immobilization [39]. An advantage of this approach is that the direct adsorption of proteins on gold can be a quick method for producing a good coating of the surface transducer [39–42]. Indeed, according to Cullen et al. [41] 5 min of contact between the biomolecules and the metallic surface can lead to 75% coverage. Nevertheless, this process is rarely used because of the numerous drawbacks associated with it, including irreproducibility of receptor binding, instability of the receptor coating and the possibility that this non-specific, direct interaction with the metal can alter the structure and biological properties of the receptor biomolecules. All these disadvantages have led to the investigation of new techniques involving a stable and specific receptor biomolecule immobilization that also allow reproducible analysis.

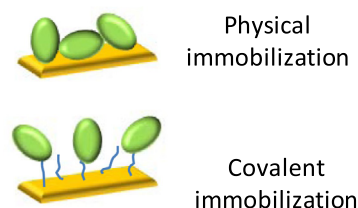


Fig. 7. A simplified representation of the two main approaches for biomolecule immobilisation on a gold substrate.

#### 4.1.2. Covalent immobilization of receptor biomolecules on the gold substrate

Chemical immobilization involves the formation of a strong covalent linkage between the receptor and the sensor surface, which improves not only the uniformity and the density of the sensitive layer but also the overall reproducibility.

**4.1.2.1. One-step receptor immobilization.** Instead of non-specifically adsorbing a biomolecule directly on the gold surface, it is also possible to exploit existing functional groups within the receptor biomolecule or to modify the biomolecule to allow it to form a specific, covalent self-assembled monolayer (SAM) on the gold surface. Self-assembled monolayers (SAM) are organized layers of amphiphilic molecules. To obtain long range molecular organization, the SAM reagents are usually constituted of a long alkyl chain to allow for intermolecular hydrophobic interactions to drive assembly. The resultant monolayer is stable, orderly and dense. The covalent bond between gold and sulfur, usually mediated through the sulfhydryl (SH) functional group in thiols, has been used extensively in the SAM functionalization of gold surfaces for sensing and molecular recognition [43]. The use of native thiols (e.g. from cysteine residues) within protein-based receptors is one option for SAM formation. However, this could disrupt overall protein structure and affect binding. Chemical modification of the receptors with pendant thiol groups has been effective in leading to SAM formation with a minimum of impact on binding efficiency [44]. This is particularly true in DNA based receptors, such as aptamers, as pendant thiol functional groups can be incorporated easily during automated solid phase synthesis of the sequence [45]. In our previous work, we immobilized 5'-alkanethiol-modified aptamers [46] to allow for one-step SAM formation on the gold substrate.

More recently, a new approach to direct receptor immobilization has been investigated using phenyldiazonium salts. The strategy of grafting phenyl radicals stemming from diazonium salts onto a surface was implemented for the first time in 1992 by Delamar et al. [47]. It consists of an electrochemical reduction of the diazonium salt in an aprotic environment. This treatment allows the formation of a covalent bond between the phenyl group and the metallic surface as represented in Fig. 8. This approach is very interesting because of its efficiency for a wide range of applications [48–50], its simplicity, its speed and its good grafting ratio of phenyl layers [51]. This diversity of use is due to the possibility of incorporating various functional groups into the para-position of the diazonium group.

The direct coupling between biomolecules and diazonium salts was, at first, realized with oligonucleotides. A DNA sequence [52] was functionalized by 4-aminobenzyl amine and electrografted on the surface, allowing the formation of a stationary phase for the hybridization with a DNA sequence target. This approach is typically used for *in situ* modification of electrode surfaces for sensing, thus it was not considered for this fiber application.

**4.1.2.2. Two-step receptor immobilization.** In this approach, the surface of the transducer is first modified with a bifunctional SAM which is then able to react with a functional group on the receptor

biomolecule in the second step. Bifunctional molecules used for SAM formation in this approach carry the thiol group (for the case of gold) for surface interaction, and other functional groups at the other end conferring new chemical reactivity to the surface [53–54].

Proponents of this method stress that the use of an intermediate organic layer helps to maintain the specific recognition properties of the receptors [55]. Several possibilities are employed for the bimolecular immobilization on the metal surface but all result in an intermediate film between the metal and the biomolecule. The intermediate film can be more or less complex according to the required properties for the biological immobilization. Thus, it can consist of either one organic monolayer like a simple SAM or of a SAM and a polymer film.

Whatever the intermediate film chosen for immobilizing a biomolecule (monolayer or polymer), it is necessary to have certain functional groups present in the film structure. These functional groups can be classified in two types. They can be reactive groups (e.g. epoxy) that can react spontaneously with some functional groups present on the receptor biomolecule. It can also be chemical groups (e.g. OH, COOH, NH<sub>2</sub>) in the intermediate film that require chemical activation in order for them to form a conjugate with the nucleophilic sites of the biomolecules. Table 1 shows some common chemical reactions used for biomolecule immobilization.

Additionally, SAMs are generally used as an intermediate layer when functionalizing a metallic substrate with a polymer film. As a consequence, the coupling reactions presented in Table 1 can also allow the immobilization of an intermediate polymer film to further isolate the biomolecules from the transducer surface and facilitate the access to the receptors. Many polymers have been studied for biomolecule immobilization, e.g. poly(acrylic acid) [64] and poly(vinylpyrrolidone) [65]. The immobilization of all these polymers can be realized by various techniques of grafting (“grafting onto” [66], “grafting from” [67]). As it is possible to control the thickness of the polymer films by “grafting from”, only this method will be described here. Fig. 9 sketches the proof of principle of the method either from an initiator immobilized on the surface (A) or from a vinyl compound (B).

The “grafting from” technique requires several steps. First, the initiator (or the vinyl compound) is immobilized on a surface functionalized by a monolayer, and then the polymerization is made from the surface resulting in a polymer film anchored on the transducer surface. When a vinyl compound is used, it is necessary to add an initiator on the solution. In this case, the polymerization is made at the same time from the surface and in the solution. After the immobilization of the polymer film, this can be used to graft biomolecules thanks to its reactive functional groups or after their activation by coupling molecule (cf. Table 1).

#### 4.2. Aptamer functional coatings

The choice of biomolecule for the specific recognition layer can depend on the desired application. Based on the advantages described in Section 1, aptamers were chosen as the specific receptor of choice for our fiber surfaces. Aptamers have been developed for a wide variety of molecular targets, ranging from small organic

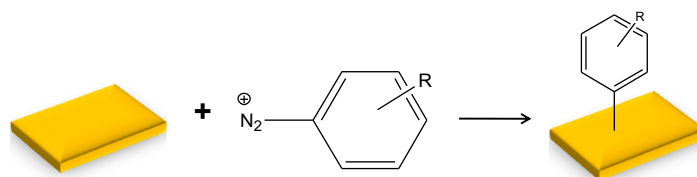
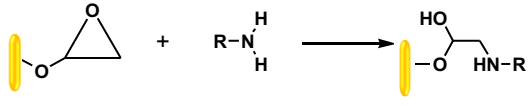
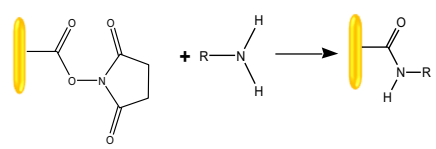
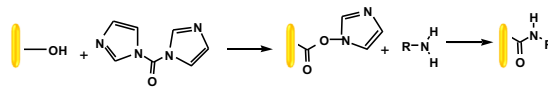
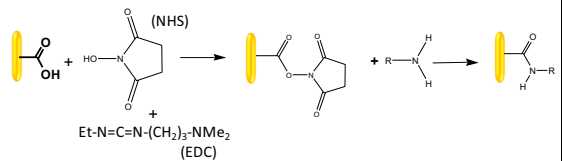


Fig. 8. Immobilization of a diazonium salt layer on a metallic surface.

**Table 1**  
Commonly used coupling reactions for immobilizing an organic layer or a biomolecule onto a surface. Note that the reactive groups are interchangeable, i.e. in Reaction (1), the amine group could be on the surface and the receptor biomolecule could be labeled with an epoxy group.

	Chemical reactions	Ref.
Reactive groups		[56-57]
		[58-59]
Activating molecule		[60-61]
		[62-63]

<sup>1</sup> EDC : ethyl(dimethylaminopropyl) carbodiimide

<sup>2</sup> NHS : N-Hydroxysuccinimide

molecules to supramolecular complexes such as viruses or cells. The Aptamer base [68] is a repository for aptamer information, where researchers can see if an aptamer for a target of interest has already been selected and find both the sequence and affinity

of that aptamer (<http://aptamerbase.semanticscience.org>). Of course, if no aptamer has been developed for a target of interest, one can use the SELEX procedure [15,69–70] to screen for binding sequences.

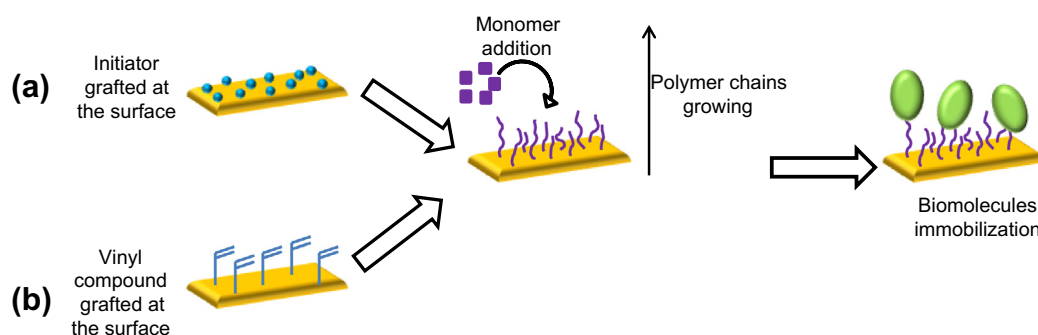


**Fig. 9.** Possible processes for the immobilization of polymer films by the “grafting from” technique. (a) and (b) refer to two possible mechanisms to initiate the grafting.



Once the DNA or RNA sequence of an aptamer is known, relatively large amounts of the aptamer can be synthesized by automated solid phase synthesis on a DNA synthesizer. [19] As described in [20], a wide range of chemistries is available for sensor surface modification. Aptamers can be synthesized with any number of functional moieties at many locations. Depending on the desired chemistry for surface attachment, modified phosphoramidites (synthetic nucleic acid building blocks) can be incorporated at precise locations in the aptamer sequence. Commercial companies such as Glen Research (<http://www.glenresearch.com/index.php>) and Chem Genes (<https://www.chemgenes.com/>) provide a range of phosphoramidites for this purpose. If a DNA synthesizer is not available, custom DNA/RNA synthesis companies are available to prepare the modified sequence. Companies such as IDT (<http://www.idtdna.com/site>) and Sigma Genosys (<http://www.sigmaaldrich.com/canada-english/sigma-genosys-canada/custom-dna-synthesis.html>) can prepare aptamers with the more routine modifications.

For our sensing application, we chose to look at the thrombin binding aptamer, a fifteen nucleotides long sequence composed entirely of guanine and thymine (5'-GGT TGG TGT GGT TGG-3') [71]. It folds into a G-quadruplex structure and interacts with  $\alpha$ -thrombin, an important enzyme in the blood-clotting cascade, in its fibrinogen-binding exosite [72]. The aptamer was synthesized on our Bioautomation Mermade Automated DNA synthesizer with a 6-mercaptohexyl (an alkyl thiol) group at the 5'-end of the sequence using a 1-O-dimethoxytrityl-hexyl-disulfide,1'-[(2-cyanoethyl)-(N,N-diisopropyl)]-phosphoramidite purchased from Glen Research.

#### 4.3. Confirmation of biomolecule immobilization

Secondary confirmation of both the receptor immobilization onto the sensor surface, and target-receptor binding, is always helpful when troubleshooting biosensor preparation and application. Techniques such as radiolabelling [73], Fourier Transform Infrared Spectroscopy [74] have found common use in this area. Fluorescence microscopy and confocal laser scanning microscopy

have been used to confirm protein binding to alkanethiols on gold [75], and in monitoring fluorophore-tagged thiols deposited on surfaces [76,77], thus confocal microscopy was a good candidate for further confirmation of the attachment of thiolated aptamers to the fiber surface. Other types of microscopy can be used to examine the sensor surface before and after target binding to help correlate sensor signal to surface coverage. Atomic force microscopy (AFM) is a powerful technique that can detect nanoscale changes to the sensor surface, thus it was chosen for our fiber analysis after protein binding experiments [78].

## 5. Interrogation of the sensing device

One of the unique features of this system is that it operates at near infrared wavelengths between 1510 and 1620 nm, where standard single mode fibers perform best. Because of this, the interrogation of the devices can be carried out with a variety of instruments, tools, and methods developed for the telecommunications industry.

### 5.1. Instrumentation

Changes in the optical properties of these devices are determined quantitatively by measuring the amount of power transmitted through the TFBG as a function of wavelength, and then by following changes in one or several narrowband attenuation dips (the “resonances”) corresponding to coupling of the core mode light into selected cladding modes. The interrogation techniques most often used to measure the transmitted amplitude spectra of TFBGs can be classified into two categories: those using a broadband optical source and an optical spectrum analyzer and those combining a tunable laser and a photodetector. The second approach is usually cheaper, faster (measurement time of the order of 1 s to cover a 100 nm wavelength range) and more accurate (1 pm of uncertainty on the wavelength value). In our experiments, we work with a Micron Optics (model si720) fiber grating interrogator, an instrument that includes a tunable laser and a photode-

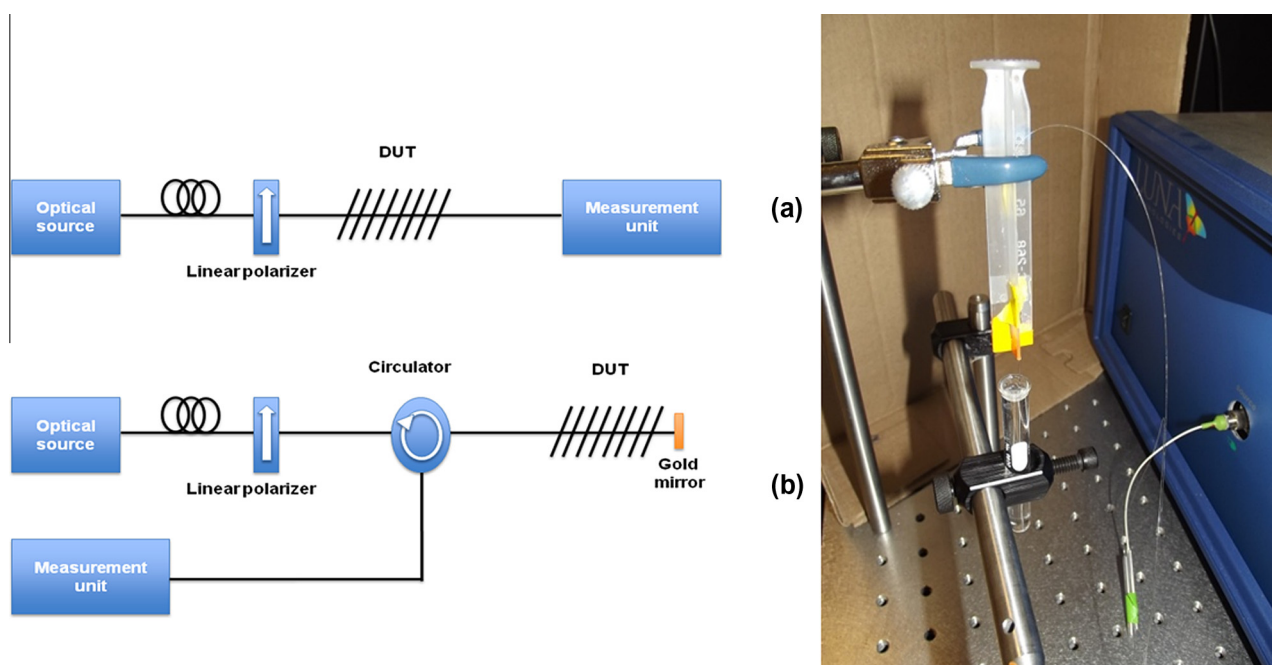


**Fig. 10.** Two possible connection configurations to interrogate TFBGs: (a) transmission mode; (b) reflection mode. The photograph shows a reflection configuration that uses the LUNA instrument (which contains all the necessary optics): the fiber is connected into the instrument at one end and inserted in a test tube at the other end.

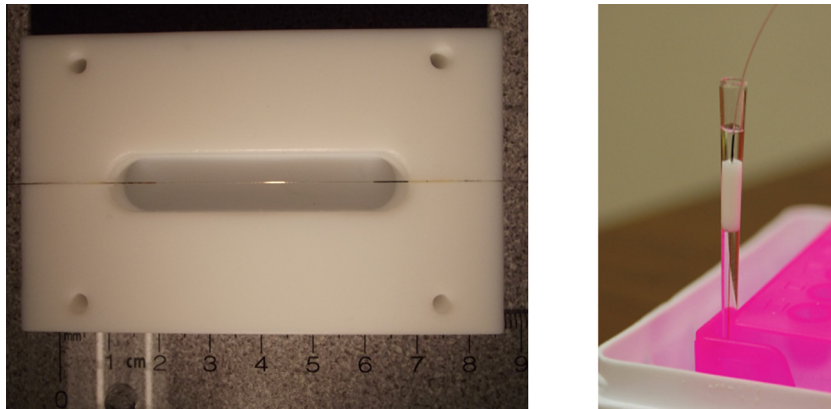


Fig. 11. On the left, a typical sensing cell in transmission mode. On the right a reflective sensor immersed in a micro test tube.

detector in a single device, as well as several data processing tools. As the polarization of the input light plays a crucial role in the interrogation process of TFBGs that are metal-coated for SPR applications, a linear polarizer is used upstream of the TFBG. Again there are several options available, all with compatible fiber inputs and outputs. We use a JDSU Polarization controller (Model PR2000), but simpler manual polarizers such as the OZ Optics FPR-1550 can be used. More sophisticated (and costlier) instrumentation that includes the polarization control with the tunable laser is available from JDSU (SWS OMNI system) and LUNA Innovation (Optical vector analyzer (OVA) model 5000 or CTe). These instruments measure the optical transmission of devices for several orthogonal polarization states at each wavelength. From these measurements, the polarization dependent loss (absolute magnitude of the total power variation for all possible input polarizations) and the minimum and maximum transmission values can be extracted easily using Jones Matrix or Mueller Matrix calculations [79]. In the case of the LUNA OVA, the latter data is available in real time during sensor interrogation (at a refresh rate of 1 Hz). All the instruments and optical components used are readily available and they are all provided with standard optical fiber connectors to which our devices are simply connected (see Fig. 10 for instance).

## 5.2. Sensing system layout

A straightforward interrogation technique for gold-coated TFBGs consists in measuring their transmitted amplitude spectrum

with linearly polarized light, as sketched in Fig. 10a. As discussed in Section 2, the angle of the input state of polarization is optimized to generate the surface Plasmon resonance. The sensor is therefore kept straight and the connecting optical fibers are maintained strain-free to avoid undesired polarization instabilities. The configuration in reflection (Fig. 10b) is more convenient to use in practice, as the sensor locates on the fiber tip and can therefore be inserted in very small volumes. Also, the probe is inherently straight and strain free. To work in reflection, two additional devices are required: an optical circulator that collects the reflected amplitude spectrum and a broadband mirror (most often a thin gold coating deposited on the cleaved fiber tip) that maximizes the end fiber reflection. It is worth mentioning that in the absence of a reflective coating at the fiber tip, the end fiber reflection (so-called Fresnel reflection) is only 4% in air, and less than 0.5% in liquids.

In the results shown in this paper the sensor is used in transmission mode. It is fixed with help of UV-sensitive adhesive in a plastic cell designed specifically for the biosensing tests (Fig. 11). The fiber containing a typical 0.5–1 cm-long grating is immersed in a carved out indentation at the surface of the cell (fiber ends are glued into slots at each end of the cell so that the grating lies straight, under the surface of the liquid). After the installation of the grating, the immersion of the sensor is conducted at the beginning of each test using a pipet adding on average 600  $\mu\text{L}$  of fluid (potential microfluidic variants are described in the conclusion). A glass slide on top of the cell prevents evaporation during experiments. In between experiments, various rinsing steps are carried

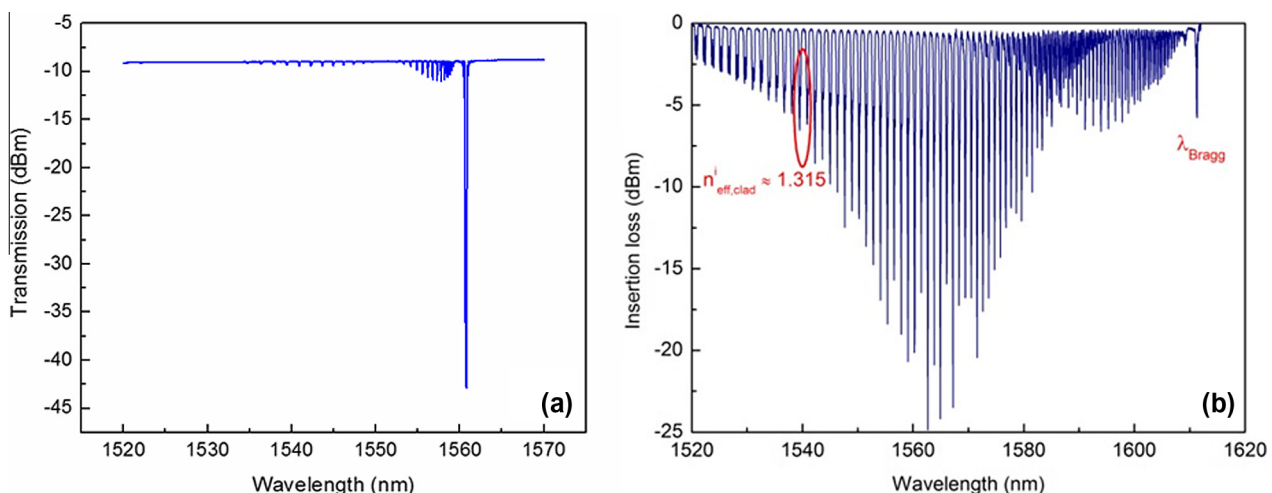


Fig. 12. Typical transmitted spectrum of 2 cm long un-tilted FBG (a) and  $10^\circ$  TFBG (b).

out as described in detail in Section 5.4 to ensure that concentration levels are accurate for all tests. We do not use temperature control thanks to the inherent temperature insensitivity of our interrogation scheme. Finally the fluid in the cell is stirred by a tiny magnetic bar located on the bottom of the cell, under the grating. For *in situ* testing, the reflective configuration is used and the sensor can be immersed directly into the fluid of interest (Fig. 11). The reflective configuration also makes it easier to immerse the sensor into various solutions of interest and to rinse it between experiments (Fig. 10). The transmission cell must be filled and rinsed carefully (manually at the present time, see Section 7 for a future microfluidics implementation).

5.3. Typical measured responses

Fig. 12a depicts the typical transmitted spectrum of a 2 cm long uniform and un-tilted FBG. A single strong rejection band centered on the Bragg wavelength near 1560 corresponds to light that is reflected backwards inside the core at that wavelength only. The use of single mode fiber ensures that there is only one such resonance. Apart from very small cladding mode resonances, light at all other wavelengths is transmitted through the grating without loss by the single mode guided by the core. With tilted grating planes, as shown on Fig. 12b for the transmitted spectrum of a 2 cm long 10°-tilt TFBG, the spectrum changes drastically and several tens of strong cladding mode resonances appear on the short wavelength side of the Bragg resonance (near 1610 nm in this case, as determined by the periodicity of the grating). As discussed earlier, when core-guided incident light at one of these resonance wavelengths encounters the grating, a large fraction (typically 90% and above) of the light intensity is coupled to a well-defined group of cladding modes (i.e. guided by the cladding of the fiber instead of the core) that is characterized by a specific value of effective refractive index, for instance  $n_{eff,clad,i}$  for the  $i$  mode. According to the phase matching relationship provided in Section 2, the group of modes whose resonance is close to 1538 nm (inside the red oval on the graph) have effective refractive index values, near 1.315, which is the refractive index of pure water at these wavelengths. When the effective refractive index of a cladding guided mode becomes equal or lower than the refractive index of the medium outside the guiding boundary, confinement is lost and the light is allowed to radiate out from the fiber. In the case of Fig. 12b, if the grating is immersed in water the resonances at wavelengths shorter than 1538 become strongly attenuated because the

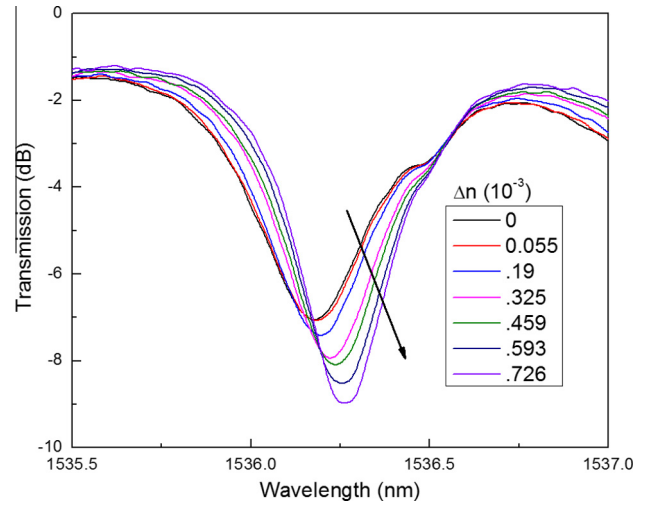


Fig. 14. Evolution of the most sensitive resonance ( $\lambda_s$ ) for a sensor immersed in a mixture of ethanol and water to increase the refractive index by  $0.726 \times 10^{-3}$  (adapted from Ref. [30]).

corresponding modes are no longer guided by the cladding water interface. Modes with resonance wavelengths close to but still larger than 1538 remain guided but very weakly and their evanescent field penetrates the outer medium over a thickness of several wavelengths. The wavelength at which modes cease to be guided is called the cut-off wavelength, and resonances just above that point are the most sensitive to SRI changes [26]. Basically, the resonances close to cut-off shift toward longer (shorter) wavelengths as the SRI increases (decreases) as a result of the large penetration of the mode fields in the surrounding medium. For resonances with wavelengths further away from the cut-off, the modes are increasingly confined into the cladding and their SRI sensitivity decreases accordingly, eventually reaching absolute insensitivity for the core mode resonance at the Bragg wavelength. The spectra shown in Fig. 12 illustrate the difference brought about by tilting the grating planes of an FBG but in this case no polarization control was used.

As noted in Section 2, the optimum use of the TFBG-SPR sensor requires linearly polarized input light, oriented along the tilt plane. With ASE sources this is achieved by inserting a polarizer in the input path and by rotating it until the resonance amplitudes of each group of modes is maximized. The two orientations thus obtained

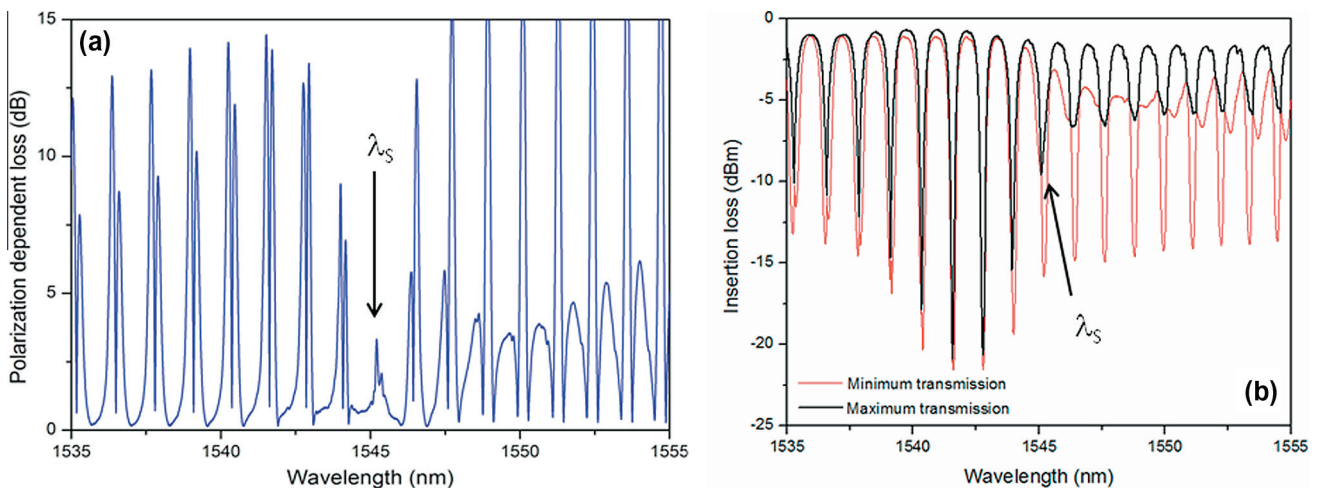


Fig. 13. PDL spectrum (a) and minimum/maximum transmission spectra (b) for a 50 nm gold-coated 10° TFBG immersed in water.

correspond to P- and S-polarized input light. This “search” is made necessary by the fact that it is not possible to predetermine the correct input polarization since we are using non polarization maintaining fiber. Once the correct angles are found, they do not change with time, as long as all the fibers in the beam path are not moved. Typical resulting spectra were already shown in Fig. 4. When using the OVA or SWS systems the situation becomes much simpler: these systems automatically generate polarization dependent data as noted in Section 4.1 and results can be expressed either as Polarization Dependent Loss (PDL defined as the difference in dB between the maximum and minimum transmission over all possible polarization states at each wavelength) as in Fig. 13a or as min/max transmission curves (i.e. a set of two transmission curves corresponding to the minimum and maximum transmission at each wavelength) (Fig. 13b), for the same data set.

#### 5.4. Interrogation methodology for biochemical recognition experiments

The methods described in the previous Section apply to all situations where the TFBG-SPR is used to measure changes in permittivity occurring at and near the surface of the gold layer. In the particular case of biochemical experiments, those changes can be very small (order of  $10^{-3}$  or less in refractive index) and occur over very thin layers (from tens of nm to a few  $\mu\text{m}$ ). In such cases the main SPR envelope shifts by very small amounts (as small as 1–5 pm) so the interrogation technique must proceed as follows:

1. Record a reference spectrum for S-polarized light in the medium where the experiment is conducted (often a saline buffer solution).
2. Record a reference spectrum for P-polarized light in the same medium, by rotating the linear input state of polarization by 90°.
3. Compare both spectra to unambiguously locate the high sensitivity resonance ( $\lambda_S$ ) on the short wavelength side of the SPR maximum. This would be the resonance near 1545 nm on Fig. 13. For skilled users, step 1 can be bypassed as the high sensitivity resonance always locates at the same position with respect to the SPR mode [80].
4. Measure changes in the amplitude and wavelength of this resonance as a function of time following the injection of analytes in different concentrations (see Fig. 14 for instance).

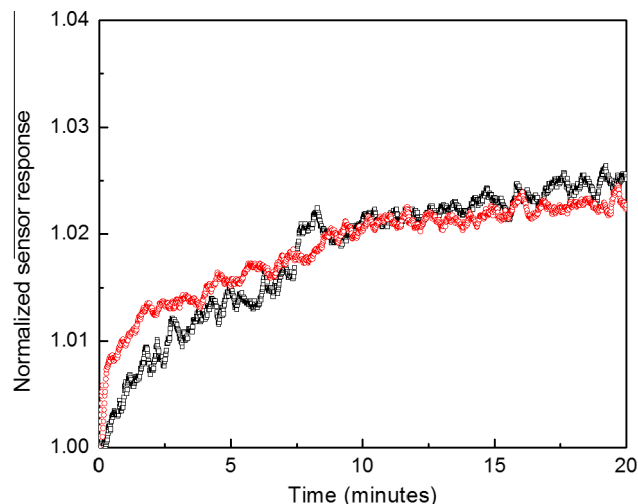


Fig. 15. TFBG-SPR response during the functionalization by aptamers (two different sensors, 10  $\mu\text{M}$  concentration of aptamer in buffer).

5. Use the Bragg resonance as a reference to compensate slight optical source power fluctuations that might occur (information contained in the power level) or shifts due to ambient temperature changes (information from the wavelength: a 0.1 °C variation yields a change of the surrounding refractive index of  $\sim 10^{-5}$  and a Bragg wavelength shift of  $\sim 1$  pm).
6. Calculate the normalized change in amplitude of the most sensitive resonance as a function of time during the binding reactions (Fig. 15 shows some typical responses).

Proceeding in this manner ensures that the maximum information can be extracted from the sensing system, with the lowest possible noise. In practice, automated means can be used to track the position of several resonances (each within a wavelength window predetermined from test runs of a particular experimental situation) so that the wavelength position and minimum transmission of the important resonance can be corrected in real time (basically by measuring all wavelengths relative to the position of the Bragg resonance and all power levels relative to the level observed on the long wavelength side of the Bragg resonance). Calibration of the sensors for absolute values of SRI can be carried out by immersing them into liquids of precisely known refractive index as described in [32], but this is not normally necessary as most biochemical binding experiments require only relative quantitative data between different molecules or concentrations.

## 6. Preparation and application of a protein aptasensor

In this section we outline the detailed experimental conditions for the preparation and the testing of the “aptasensor”. The reagents used for the immobilization of the aptamers on the optical surface depend on the desired approach to receptor immobilization. Here are detailed protocols for our approach to aptamer immobilization and sensor testing. Experimental details for the other techniques presented in Section 4 can be found in Refs. [71,72].

### 6.1. Materials

All buffer solutions described herein were prepared using doubly deionized water from a Milli-Q water system (ThermoFisher). All DNA phosphoramidites and modifiers were purchased from Glen Research. Bovine Serum and Bovine Serum Albumin were purchased from Sigma Aldrich. Bovine serum solution for testing was prepared as a solution of 50% Serum: 50% Tris Buffer (50 mM Tris pH 7.4, 1 mM  $\text{MgCl}_2$ , 140 mM NaCl, 5 mM KCl). The thiolated thrombin aptamer, DNA sequence HS-( $\text{CH}_2$ )<sub>6</sub>-5'-GGT TGG TGT GGT TGG - 3' was synthesized on a MerMADE 6 DNA synthesizer (Bioautomation Corporation). The sequence purification was conducted using Clarity QSP Cartridges (Phenomenex). The DNA was dissolved in “DNA buffer” (5 mM phosphate, 100 mM  $\text{MgCl}_2$ , 50 mM NaCl). The mass of the DNA sequences were confirmed by ESI-MS and the Ellmann’s test [81] was conducted to test for presence of the 5'-thiol group prior to binding. Human alpha-thrombin protein was purchased from Hematologic Technologies Inc. The protein was aliquoted as needed and dissolved in “Protein Buffer” (50 mM Tris pH 7.4, 1 mM  $\text{MgCl}_2$ , 140 mM NaCl, 5 mM KCl). The sequences used for the confocal microscopy experiments were purchased from Alpha DNA (Montreal). In this case, the thrombin aptamer sequences possessed the 5'-thiol C6 modifier, as well as a Cyanine 3 (Cy3) dye modifier at the 3' end, making the overall sequence 5'-HS-( $\text{CH}_2$ )<sub>6</sub>-GGT TGG TGT GGT TGG-Cy3-3' (herein called Cy3 DNA).

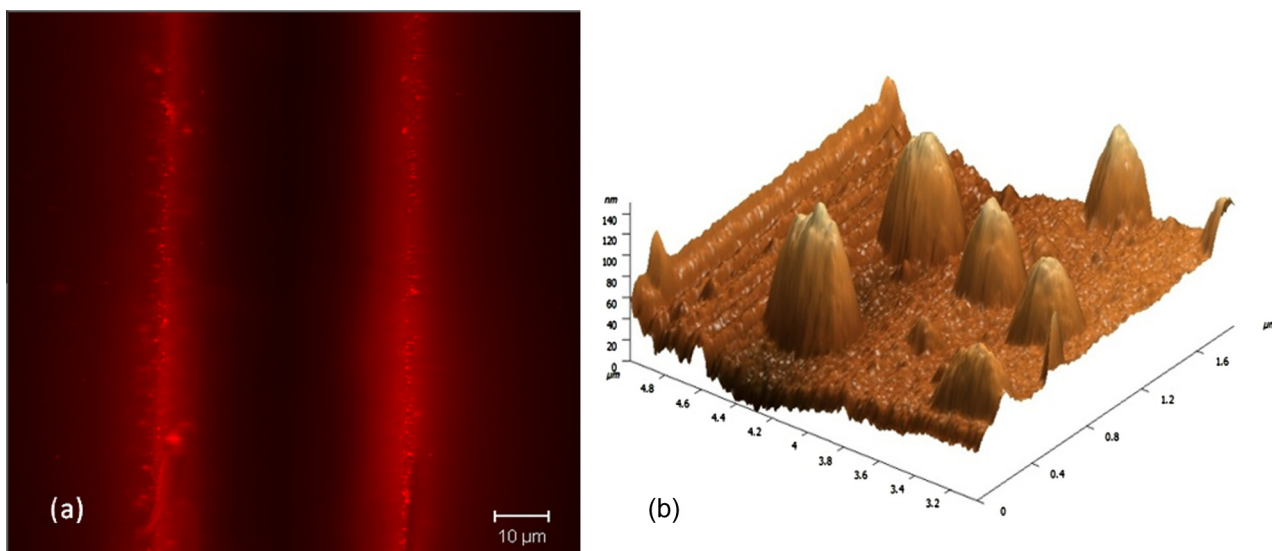


**Fig. 16.** (a) Confocal image of sensor with fluorescently labeled aptamers [46]; (b) AFM image of sensor after protein attachment (concentration of 5  $\mu\text{M}$ ).

### 6.2. Direct deposition of SH-modified aptamers

This is achieved following 4 main steps

- (1) Prior to surface modification, the gold surface is cleaned to remove organics and other potential interferents that could affect SAM formation. While cleaning by polishing [82], ozone [83], or etching [84] have all been suggested for electrochemical sensing using gold, in our experience a simple rinsing with ethanol and then de-ionized water was sufficient for our purposes.
- (2) The thiol-modified aptamer solution with the desired concentration is deposited on the gold surface for 120 min. The aptamer is dissolved in an appropriate buffer (we used our “DNA buffer”). Prior to deposition, confirmation of the presence of the 5'-thiol group can be done using the Ellmann's test as shown in reference [81]. The deposition of the aptamer can be tracked by monitoring the relative change in SPR signal during the deposition process. We observed that deposition occurs quickly over the first 5–10 min, and that aptamer concentrations in the range of 10–20  $\mu\text{M}$  are high enough to saturate the surface. Fig. 15 shows the amplitude of the most sensitive resonance (relative to its value, in dB, at the beginning of the aptamer attachment process, for two different experiments (and sensors).
- (3) At the end of the deposition process, a 20 min rinse of the sensor is done with water and then “DNA buffer”. If desired, this can also be monitored in real time by SPR.
- (4) At this stage, if fluorescence microscopy will be used for confirmation, the fiber should be rinsed thoroughly (until washings are colorless) to remove any unbound aptamers. The fiber can then be imaged while mounted on microscope slides in a solution of 50% glycerol in water. Fluorescently-labeled aptamer using a common fluorescent dye, Cy3, attached at the 3'-end of the aptamer can be used for these experiments.

For our experiments, all images were collected on a confocal microscope, the Zeiss LSM510 with a Plan-Apochromat 63 $\times$ /1.4 Oil Dic objective with LP950 filter, with an excitation wavelength of 550 nm and an emission wavelength of 570 nm. A control fiber that has been incubated in dye-labeled aptamer lacking the 5'-thiol

group, and hence unable to form the SAM on the surface, can account for any non-specific binding of the aptamer to the fiber surface. The presence of fluorescence on the surface of the fiber (Fig. 16a), over and above any detected in the control, is confirmation of successful aptamer immobilization. However, once protocols are well established, the use of labeled aptamers is not necessary for our aptasensor.

### 6.3. Thrombin detection

The functionalized sensor can now be exposed to target protein (Human  $\alpha$ -thrombin) at different concentrations in protein buffer, for at least 20 min incubation time. Again, results from target binding can be recorded in real-time. In a similar fashion to the DNA immobilization step, the addition of thrombin shows a rapid change in SPR signal over the first 10 min of immersion, after which it begins to stabilize, as shown in Fig. 17 for a concentration of 5 mM of thrombin. A 20 min rinsing step with protein buffer is recommended at the end of each experiment. It is inter-

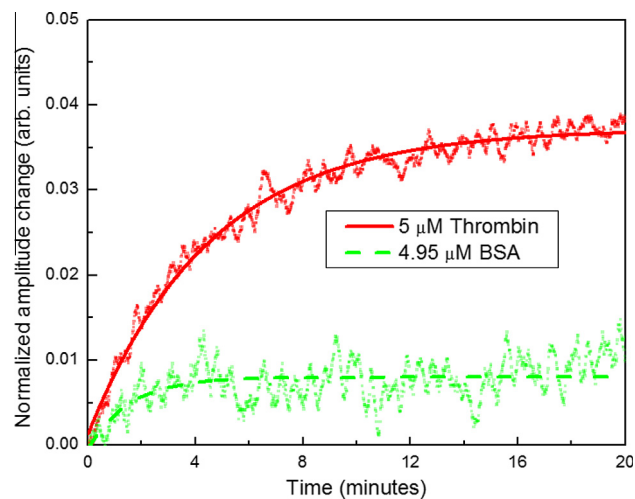


**Fig. 17.** Aptamer functionalized TFBG-SPR response in 5  $\mu\text{M}$  concentrations of thrombin and BSA. Dots represent the raw sensor response of the most sensitive resonance amplitude and straight lines are exponential fits to the data.

esting to note that proteins do not attach regularly on the sensor surface but rather form isolated clusters (Fig. 16b). This granularity does not perturb our measurement because the transmission of our device reflects the average impact of the additional molecules over the whole length of fiber surface that covers the grating.

In order to validate that the signal is generated due to a specific interaction, a control protein should also be tested. Bovine Serum Albumin (BSA) was chosen as control in our experiments: the choice of BSA arose from the fact that BSA is typically used as a control for thrombin aptamer studies [85]. It is much larger than thrombin (67 kDa compared to 37 kDa for thrombin), though, and as a result there is a greater possibility of nonspecific interactions with the fiber surface. Fig. 17 shows a one order of magnitude difference in the sensor response to identical concentrations of Thrombin and BSA. In a more detailed paper about these particular experiments, our data revealed that detection of thrombin at concentrations as low as 0.1  $\mu\text{M}$  are possible and that a sizeable difference in the signals of 0.1  $\mu\text{M}$  thrombin protein, of 5  $\mu\text{M}$  BSA, and of 5  $\mu\text{M}$  pepsin (another non-specific target) can be seen in as little as 10 min [46]. In the same paper, more complex solutions were tested in order to evaluate the sensor's versatility and potential applicability in a real-world setting. We chose bovine serum as it contains a high concentration (60 mg/mL) of nonspecific proteins and would more closely mimic testing in a true biological sample. Although a strong non-specific signal is present in the serum, we found that this sensor platform can be used in complex media such as serum just as effectively as simple media such as buffer. All results above represent normalized amplitude evolution, relative to the amplitude at the beginning of each cycle of experiments (in dB). This method provides a LOD for thrombin of 22 nM, based on three times the noise level in our system [46,86].

Finally, the attachment of the target protein to the fiber surface can also be confirmed using atomic force microscopy. AFM images were collected on an Ntegra system using a SFC050LNTF AFM Head on an inverted microscope (Olympus IX71). After target immersion, the fibers were rinsed with Milli-Q water. All sample micrographs were collected in air on the dry samples. Fig. 16b reveals that the sensor surface has many new structural features after target exposure that are not present on the aptamer modified surface alone, in agreement with the change in SPR noted upon target incubation.

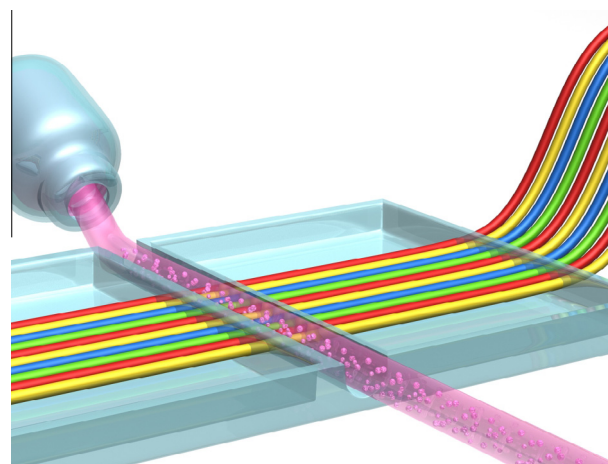


Fig. 19. Artist conception of a multiplexed TFBG-SPR sensors embedded across a microfluidic channel.

#### 6.4. $K_d$ analysis

The dissociation constant ( $K_d$ ) is a parameter used to characterize the binding strength between two interacting molecules. The last result to be presented here deals with the ability of the SPR-TFBG to determine  $K_d$  constants during *in situ* measurement of biomolecular interactions. The  $K_d$  value can be determined with an analyte “Ladder” test. The sensor functionalized with the aptamers is immersed in successive solutions of increasing concentrations of the target. Fig. 18 shows an exemplary TFBG-SPR signal response during a “Ladder test” for the aptamer-Thrombin system [46].

In Fig. 18 the successive steps of the ladder are: (1) Milli-Q water; (2) DNA buffer; (3) aptamer, 20  $\mu\text{M}$ ; (4) thrombin, 0.1  $\mu\text{M}$ ; (5) thrombin, 0.5  $\mu\text{M}$ ; (6) thrombin, 1  $\mu\text{M}$ ; (7) thrombin, 5  $\mu\text{M}$ ; (8) protein buffer; (9) regeneration in 0.2 M of  $\text{Na}_2\text{CO}_3$ . The results confirm that the specific interaction between the protein and the sensor leads to a signal increase after each new higher concentration, and that an increase of the SPR signal remains after a final protein buffer wash. The surface is thus modified by the immobilization of the target protein. The inset in the figure illustrates the relationship between normalized SPR signal change

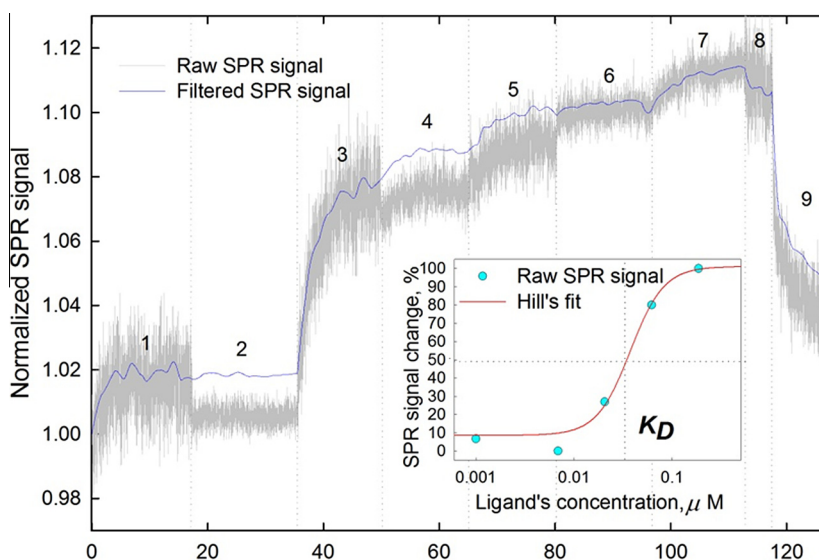


Fig. 18. Normalized amplitude of the TFBG-SPR aptasensor as a function of time, for increasing concentrations of thrombin (details in the text) (from [46]).

and thrombin concentration, from which  $K_d$  can be estimated [87]. Our results indicate a value of  $40 \pm 1$  nM, within the bounds of  $K_d$  values found for the same aptamer-protein system in solutions (between 20 and 400 nM [71,88]). While it is well-known that a covalent immobilization of protein on metallic surfaces may alter the binding characteristics of the biological system [89], the obtained results confirmed that the aptamer affinity was unaffected by immobilization on the sensor surface and that the sensor was able to detect target binding across the relevant thrombin concentrations.

## 7. Conclusions

Fiber-based biochemical sensors fill an increasingly well-defined niche in the sense that they do not require elaborate light management schemes to probe molecules and materials: light remains guided in the fiber from source to detector, apart from localized probe regions where it interacts with the immediate surroundings of the fiber. This feature is the dominant factor in making such sensors less expensive to fabricate and to use than conventional biosensors (especially those based on surface plasmon resonance and resonant waveguide gratings). However this comes with two main inconveniences: a higher (worse) limit of detection and the impossibility to scale up toward massively parallel testing.

The TFBG-SPR devices that we are proposing here address the first issue by combining the surface plasmon resonance effect with the grating-based approach in a single sensor that keeps all the advantages of the fiber solution. The underlying fiber grating provides a fine comb of high Q-factor resonances that probe the SPR envelope and allow an order of magnitude improvement in the determination of the SPR shifts under biochemical interactions at the fiber surface. We have shown that we can separately excite resonances that enable SPR effects and resonances that do not (which can serve as reference channels). The sensor also provides absolute *in situ* temperature information, from the wavelength position of resonances that are isolated from the outer surface. All of this additional information can be used to average out noise and to eliminate many cross-sensitivity factors. We have also demonstrated that aptamer based bio-recognition molecules are compatible with the gold coatings that we use to generate SPR effects on fibers and provided detailed process steps to implement them for typical sensing experiments.

Finally, the single-mode fiber that we use is compatible with a wealth of instrumentation developed for optical networks, including switch matrix devices that allow automatic interrogation of several tens of optical fibers in relatively rapid succession (on the order of one second per fiber). Therefore the multiplexing issue could be partially addressed by preparing multi-fiber sensing devices embedded in a single substrate that includes a fluidic channel across the sensing regions of the fibers (Fig. 19). In such configuration, each fiber represents one channel of the multiplexed system and the fibers are read sequentially using the switch matrix. With different surface preparations, the separate channels can be designed to capture several targets, to provide baseline reference data, or just to improve the LOD through statistical analysis of the response of multiple identical sensors. Finally, the very simple implementation proposed in Fig. 19 could be fitted with more advanced microfluidic circuitry to refresh and prepare fiber coatings individually prior to flowing unknown samples through the multiplexed sensors.

Much of the development required for the exact quantification and deployment of practical sensors based on these technologies is still in progress but it is hoped that the results presented herein will stimulate further research in this area.

## Acknowledgments

This work is financed by grants from the Natural Science and Engineering Research Council of Canada, the Canada Research Chairs program, and the Canada Foundation for Innovation. C. Caucheteur is supported by the Belgian F.R.S.-FNRS and holds an ERC (European Research Council) Starting Independent Researcher Grant (grant agreement No. 280161 – <http://hosting.umons.ac.be/erc-prosper>).

## References

- [1] H. Raether, *Surface Plasmons on Smooth and Rough Surfaces and on Gratings*, Springer-Verlag, Berlin, 1988.
- [2] J. Homola, *Surface Plasmon Resonance Based Sensors*, Springer Series on Chemical Sensors and Biosensors, Springer, Berlin, 2006. ISSN: 1612-7617.
- [3] S. Roh, T. Chung, B. Lee, *Sensors* 11 (2011) 1565–1588.
- [4] X. Fan, I.M. White, S.I. Shopova, H. Zhu, J.D. Suter, Y. Sun, *Anal. Chim. Acta* 620 (2008) 8–26.
- [5] Commercially available system examples: <http://www.biocore.com/lifesciences/index.html>; <http://www.horiba.com/scientific/products/surface-plasmon-resonance-imaging-spri/>; <http://www.corning.com/lifesciences/epic/en/index.aspx>.
- [6] J. Homola, H. Vaisocherova, J. Dostalek, M. Piliarik, *Methods* 37 (2005) 26–36.
- [7] A.V. Kabashin, S. Patskovsky, A.N. Grigorenko, *Opt. Express* 17 (2009) 21191–21204.
- [8] O.S. Wolfbeis, *Anal. Chem.* 80 (2008) 4269–4283.
- [9] B. Lee, S. Roh, J. Park, *Opt. Fiber Technol.* 15 (2009) 209–221.
- [10] F. Baldini, M. Brenici, F. Chiavaioli, A. Giannetti, C. Trono, *Anal. Bioanal. Chem.* 402 (2012) 109–116.
- [11] J. Albert, L.-Y. Shao, C. Caucheteur, *Laser Photonics Rev.* (2012) 1–26, <http://dx.doi.org/10.1002/lpor.201100039>.
- [12] J. Pollet, F. Delport, K.P.F. Janssen, K. Jans, G. Maes, H. Pfeiffer, M. Wevers, J. Lammertyn, *Biosens. Bioelectron.* 25 (2009) 864–886.
- [13] T. Schuster, R. Herschel, N. Neumann, C.G. Schaffer, *J. Lightwave Technol.* 30 (2012) 1003–1008.
- [14] A.K. Sharma, R. Jha, B. Gupta, *IEEE Sens. J.* 7 (2007) 1112–1129.
- [15] M. McKeague, M.C. DeRosa, *J. Nucl. Med. Biol.* 40 (2012) 748913.
- [16] N.K. Navani, W.K. Mok, Y. Li, *ChemBioChem* 10 (2009) 238–241.
- [17] Z. Balogh, G. Lautner, V. Bardóczy, B. Komorowska, R.E. Gyurcsányi, T. Mészáros, *FASEB J.* 24 (2010) 4187–4195.
- [18] K. Sefah, D. Shangguan, X. Xiong, M.B. O'Donoghue, W. Tan, *Nat. Protoc.* 5 (2010) 1169–1185.
- [19] J. Goodchild, *Bioconj. Chem.* 1 (1990) 165–187.
- [20] S. Balamurugan, A. Obubuafo, S.A. Soper, D.A. Spivak, *Anal. Bioanal. Chem.* 30 (2008) 1009–1021.
- [21] A. Othonos, K. Kalli, *Fiber Bragg Gratings: Fundamentals and Applications in Telecommunications and Sensing*, Artech House, 1999.
- [22] T. Erdogan, *J. Lightwave Technol.* 15 (1997) 1277–1294.
- [23] T. Erdogan, J.E. Sipe, *JOSA A* 13 (1996) 296–313.
- [24] G. Laffont, P. Ferdinand, *Meas. Sci. Technol.* 12 (2001) 765–772.
- [25] C. Caucheteur, P. Mégret, *Photon. Technol. Lett.* 17 (2005) 2703–2705.
- [26] C.F. Chan, C. Chen, A. Jafari, A. Laronche, D.J. Thomson, J. Albert, *Appl. Opt.* 46 (2007) 1142–1149.
- [27] C. Chen, J. Albert, *Electron. Lett.* 42 (2006) 1027–1028.
- [28] I.M. White, X.D. Fan, *Opt. Express* 16 (2008) 1020–1028.
- [29] Y.Y. Shevchenko, J. Albert, *Opt. Lett.* 32 (2007) 211–213.
- [30] Y.Y. Shevchenko, C. Chen, M.A. Dakka, J. Albert, *Opt. Lett.* 35 (2010) 637–639.
- [31] C. Caucheteur, C. Chen, V. Voisin, P. Berini, J. Albert, *Appl. Phys. Lett.* 99 (2011) 041118.
- [32] C. Caucheteur, Y.Y. Shevchenko, L.-Y. Shao, M. Wuilpart, J. Albert, *Opt. Express* 19 (2011) 1656–1664.
- [33] V. Voisin, C. Caucheteur, P. Mégret, J. Albert, *Appl. Opt.* 50 (2011) 4257–4261.
- [34] P.J. Lemaire, R.M. Atkins, V. Mizrahi, A.W. Reed, *Electron. Lett.* 29 (1993) 1191–1193.
- [35] S. Hrapovic, Y. Liu, G. Enright, F. Bensebara, J.H.T. Luong, *Langmuir* 19 (2003) 3958–3965.
- [36] H. Tazawa, T. Kanie, M. Katayama, *Appl. Phys. Lett.* 91 (2007) 113901.
- [37] I. Cordek, X.W. Wang, W.H. Tan, *Anal. Chem.* 71 (1999) 1529–1533.
- [38] A. Bialiyayeu, C. Caucheteur, N. Ahamad, A. Ianoul, J. Albert, *Opt. Express* 19 (2011) 18742–18753.
- [39] R.C. Ebersole, J.A. Miller, J.R. Moran, M.D. Ward, *J. Am. Chem. Soc.* 112 (1990) 3239–3241.
- [40] F.F. Bier, F. Kleinjung, F.W. Scheller, *Sens. Actuators B* 38 (1997) 78–82.
- [41] D.C. Cullen, R.G.W. Brown, C.R. Lowe, *Biosensors* 3 (1987) 211–225.
- [42] R.P.H. Kooyman, H. Kolkman, J. Vangent, J. Greve, *Anal. Chim. Acta* 213 (1988) 35–45.
- [43] H. Häkkinen, *Nat. Chem.* 4 (2012) 443–455.
- [44] S. Ferretti, S. Paynter, D.A. Russell, K.E. Sapsford, D.J. Richardson, *Trends Anal. Chem.* 19 (2000) 530–540.
- [45] S. Balamurugan, A. Obubuafo, S.A. Soper, R.L. McCarley, D.A. Spivak, *Langmuir* 22 (2006) 6446–6453.

- [46] Y. Shevchenko, T.J. Francis, D.A.D. Blair, R. Walsh, M.C. DeRosa, J. Albert, *Anal. Chem.* 83 (2011) 7027–7034.
- [47] M. Delamar, R. Hitmi, J. Pinson, J.M. Saveant, *J. Am. Chem. Soc.* 114 (1992) 5883–5884.
- [48] S. Betelu, C. Vautrin-UI, J. Ly, A. Chausse, *Talanta* 80 (2009) 372–376.
- [49] S. Boland, K. Foster, D. Leech, *Electrochim. Acta* 54 (2009) 1986–1991.
- [50] C. Agnes, J.C. Arnault, F. Omnes, B. Jousseme, M. Billon, G. Bidan, P. Mailley, *Phys. Chem. Chem. Phys.* 11 (2009) 11647–11654.
- [51] D. Evrard, F. Lambert, C. Policar, V. Bolland, B. Limoges, *Chem. Eur. J.* 14 (2008) 9286–9291.
- [52] T. Fujiki, S. Haraoka, S. Yoshioka, K. Ohshima, A. Iwashita, M. Kikuchi, *Int. J. Oncol.* 20 (2002) 669–679.
- [53] E. Ostuni, L. Yan, G.M. Whitesides, *Colloids Surf. B* 15 (1999) 3–30.
- [54] T. Wink, *Analyst* 122 (1997) R43–R50.
- [55] G.J. Leggett, C.J. Roberts, P.M. Williams, M.C. Davies, D.E. Jackson, S.J.B. Tendler, *Langmuir* 9 (1993) 2356–2362.
- [56] K. Nishio, Y. Masaike, M. Ikeda, H. Narimatsu, N. Gokon, S. Tsubouchi, M. Hatakeyama, S. Sakamoto, N. Hanyu, A. Sandhu, H. Kawaguchi, M. Abe, H. Handa, *Colloids Surf. B* 64 (2008) 162–169.
- [57] Y. Zheng, H.Y. Liu, P.V. Gurgel, R.G. Carbonell, *J. Membr. Sc.* 364 (2010) 362–371.
- [58] L. Garcia-Uriostegui, G. Burillo, E. Bucio, *Eur. Polym. J.* 46 (2010) 1074–1083.
- [59] Y. Liang, D.Y. Tao, J.F. Ma, L.L. Sun, Z. Liang, L.H. Zhang, Y.K. Zhang, *J. Chromatogr. A* 1218 (2011) 2898–2905.
- [60] R. Goncalves, M.C.L. Martins, M.J. Oliveira, G. Almeida-Porada, M.A. Barbosa, *J. Biomed. Mater. Res. A* 94 (2011) 576–585.
- [61] S.H. Yoshimura, S. Khan, H. Maruyama, Y. Nakayama, K. Takeyasu, *Biomacromolecules* 12 (2011) 1200–1204.
- [62] A. Hayat, L. Barthelmebs, A. Sassolas, J.L. Marty, *Talanta* 85 (2011) 513–518.
- [63] R. Jackeray, C. Abid, G. Singh, S. Jain, S. Chattopadhyaya, S. Sapra, T.G. Shrivastav, H. Singh, *Talanta* 84 (2011) 952–962.
- [64] P. Akkhat, V.P. Hoven, *Colloids Surf. B* 86 (2011) 198–205.
- [65] A.M. Telford, M. James, L. Meagher, C. Neto, *Appl. Mater. Interfaces* 2 (2010) 2399–2408.
- [66] D. Bernand-Mantel, M.M. Chehimi, M.C. Millot, B. Carbonnier, *Surf. Interface Anal.* 42 (2010) 1035–1040.
- [67] M. Li, H.M. Li, P. De, B.S. Sumerlin, *Macromol. Rapid. Commun.* 32 (2011) 354–359.
- [68] J. Cruz-Toledo, M. McKeague, X. Zhang, A. Giamberardino, E. McConnell, T. Francis, M.C. DeRosa, M. Dumontier, *Database* (2012) bas006, <http://dx.doi.org/10.1093/database/bas006>.
- [69] C. Tuerk, L. Gold, *Science* 249 (1990) 505–510.
- [70] A.D. Ellington, J.W. Szostak, *Nature* 346 (1990) 818–822.
- [71] L.C. Bock, L.C. Griffin, J.A. Latham, E.H. Vermaas, J.J. Toole, *Nature* 355 (1992) 564–566.
- [72] K. Padmanabhan, K.P. Padmanabhan, J.D. Ferrara, J.E. Sadler, A. Tulinsky, *J. Biol. Chem.* 268 (1993) 17651–17654.
- [73] E. Stenberg, B. Persson, H. Roos, C. Urbaniczky, *J. Colloid Interface Sci.* 143 (1991) 513–526.
- [74] R.M. Nyquist, A.S. Eberhardt, L.A. Silks, Z. Li, X. Yang, B.I. Swanson, *Langmuir* 16 (2000) 1793–1800.
- [75] G.E. Slaughter, E. Bieberich, G.E. Wnek, K.J. Wynne, A. Giuseppi-Elie, *Langmuir* 20 (2004) 7189–7200.
- [76] J. L. Shepherd, A. Kell, E. Chung, C.W. Sinclair, M.S. Workentin, D. Bizzotto, *J. Am. Chem. Soc.* 126 (2004) 8329–8335.
- [77] J.L. Shepherd, D. Bizzotto, *Langmuir* 22 (2006) 4869–4876.
- [78] P. Zhang, W. Tan, J. Fresenius, *Anal. Chem.* 369 (2001) 302–307.
- [79] D.S. Kliger, J.W. Lewis, C.E. Randall, *Polarized Light in Optics and Spectroscopy*, Academic Press, 1990.
- [80] C. Caucheteur, V. Voisin, J. Albert, *Opt. Express* 21 (2013) 3055–3066.
- [81] G.L. Ellmann, *Arch. Biochem. Biophys.* 82 (1959) 70–77.
- [82] J.W. Chen, X.P. Liu, K.J. Feng, Y. Liang, J.H. Jiang, G.L. Shen, R.Q. Yu, *Biosens. Bioelectron.* 24 (2008) 66–71.
- [83] C.G. Worley, R.W. Linton, *J. Vac. Sci. Technol. A* 13 (1995) 2281–2284.
- [84] N.P. Westcott, B.M. Lamb, M.N. Yousaf, *Anal. Chem.* 81 (2008) 3297–3303.
- [85] M.A. Rahman, J.I. Son, M. Won, Y. Shim, *Anal. Chem.* 81 (2009) 6604–6611.
- [86] J. Vial, A. Jardy, *Anal. Chem.* 71 (1999) 2672–2677.
- [87] W. Bode, I. Mayr, U. Baumann, R. Huber, S.R. Stone, *J. Hofsteenge, EMBO J.* 8 (1989) 3467–3475.
- [88] N. Hamaguchi, A. Ellington, M. Stanton, *Anal. Biochem.* 294 (2001) 126–131.
- [89] M. Jing, M.T. Bowser, *Anal. Chim. Acta* 686 (2011) 9–18.